Arabian Journal of Chemistry (2014) xxx, xxx–xxx

King Saud University

Arabian Journal of Chemistry

www.ksu.edu.sa
www.sciencedirect.com

ORIGINAL ARTICLE

Formation of Mn_3O_4 nanobelts through the solvothermal process and their photocatalytic property

Khalid Abdelazez Mohamed Ahmed [a,b,*], **Kaixun Huang** [c]

[a] *Department of Chemistry, Faculty of Science and Technology, Al-Neelain University, P.O. Box: 12702, Khartoum, Sudan*
[b] *Department of Chemistry, Faculty of Science and Education, Taif University, P.O. Box: 888, Postal Code: 5700, Saudi Arabia*
[c] *School of Chemistry and Chemical Engineering, Huazhong University of Science and Technology, Wuhan 430074, PR China*

Received 24 September 2013; accepted 18 August 2014

KEYWORDS

Manganese oxide;
Solvothermal;
Nanobelts;
Diphenylthiocarbazone

Abstract Hausmannite Mn_3O_4 nanobelts were synthesized from manganese acetate and potassium hydroxide precursors in the presence of melamine–ethanol–distill water via the reflux and solvothermal methods. X-ray diffraction (XRD) and Fourier transform infrared (FT-IR) spectroscopes confirm the composition of the as-prepared product. Field emission scanning electron microscopy (FE-SEM), transmission electron microscopy (TEM), selected area electron diffraction (SA-ED), high resolution transmission electron microscopy (HR-TEM) and N_2 adsorption-desorption isotherm results showed that the as-fabricated sample exhibits a nanosized belt-like crystal, single crystalline, tetragonal phase structure and high BET surface area. The effects of the reaction conditions such as melamine amount, solvent ratios and reaction time on the morphology of the products were studied. The band gap of the as-synthesized products was calculated via diffuse reflectance spectral analysis and their activity of catalytic oxidation was evaluated by degradation of diphenylthiocarbazone under visible-light irradiation. GC–MS instrument was used to monitor the temporal course of the catalytic reaction. The results showed that the degradation efficiency of diphenylthiocarbazone catalyzed by Mn_3O_4 nanobelts was higher than that which had been prepared in particle and sheet-like nanocrystals.

1. Introduction

One-dimensional (1D) inorganic nanomaterials with various shapes and morphologies, such as nanotubes, nanowires, nanorods and nanobelts generally show enhanced physiochemical applications in various areas due to their high surface to size effects and reduced dimensionality not only have been attracting a great deal of research interest in recent years,

* Corresponding author at: Department of Chemistry, Faculty of Science and Education, Taif University, P.O. Box: 888, Postal Code: 5700, Saudi Arabia. Tel.: +966 552639984.
E-mail address: khalidgnad@hotmail.com (K.A.M. Ahmed).

Peer review under responsibility of King Saud University.

Production and hosting by Elsevier

http://dx.doi.org/10.1016/j.arabjc.2014.08.014

but also they have been emerging as one of the most powerful and diverse classes of functional nanomaterials that are having a key impact on science and technology (Huang et al., 2001; Song et al., 2005; Comini et al., 2005; Mai et al., 2006; Fang et al., 2011a,b; Li et al., 2012; Peng et al., 2014). In particular, as one of the most important 1D-material structures quasi-one-dimensional nanobelts appear to have unique ability to combine a number of essential diagnostic, imaging, delivery and dosage properties and thus can be functionalized accordingly (Pan et al., 2001; Mo et al., 2002; Wang, 2004; Yu et al., 2008; Ahmad et al., 2011). Through electrical characterization, the belt-like morphology was also regarded sensitive to oxygen and environmental polluting species, like CO and NO_2 as well as ethanol for breath analyzers and food control applications due to quasi-one-dimensional structurally controlled nanomaterial with well-defined chemical composition, crystallographic structure and surfaces area (Comini et al., 2005).

One of the key concepts of material chemistry is that the properties of a material depend not only on its chemical composition but also on the method used for its preparation (Williams et al., 1984; Ahmadi et al., 1996; Xia et al., 2003; Xiao et al., 2004). With regard to Mn_3O_4 material properties, aside from their chemical composition, both nanostructures inclusive of morphology and particle size distribution play an important role for improving the surface area and reaction activity (Song et al., 2013). In order to prepare one-dimensional Mn_3O_4 nanomaterials with favorable morphology, small particle size and uniform particle size distribution such as nanorods, nanowires, nanofibers and nanotubes, various methods were utilized, including oxidation of manganese chloride by sodium hydroxide (Wang et al., 2008), solid-state decomposition of exfoliated MnO_2 nanosheets (Lee and Jung, 2012), soft chemistry templating process using a block copolymer(Du et al., 2008; Tan et al., 2011), electrospined technique (Shao et al., 2004) and hydrogen reduction of β-MnO_2 nanotubes under a H_2/Ar atmosphere (Bai et al., 2013). However, the exploration of microemulsion route for the synthesis Mn_3O_4 nanocrystals was recently attempted for preparing a poor phase of belt-like morphology (Wang et al., 2003).

The treatment of environmental pollution has become one of the most critical issues in the world. Despite the progress made in the study of semiconductor photocatalysis, it is still a challenge to obtain photocatalysts with high activity through relatively simple fabrication processes (Han et al., 2014). Until now, many kinds of advanced oxidation technologies, such as photocatalysis, wet-oxidation and catalytic ozonation were previously developed to degrade the pollution environments (Dong et al., 2009). Among different metal oxides, Mn_3O_4 materials were employed as catalyst for oxidation of methane and carbon monoxide, selective reduction of nitrobenzene, combustion of organic compounds; limitation of NO_x emission and volatile organic compounds from waste gases, decolorization of methylene blue and procion red dyes from the waste-water (Zwinkels et al., 1993; Shen et al., 1993; Grootendorst et al., 1995; Armstrong and Bruce, 1996; Baldi et al., 1998; Stobhe et al., 1999; Chowdhury et al., 2009). Therefore, besides catalytic activity, it also acts as an electrocatalyst for triiodide reduction and novel supercapacitor design performance for electrochemical energy storage (Zhang et al., 2014; Li et al., 2014).

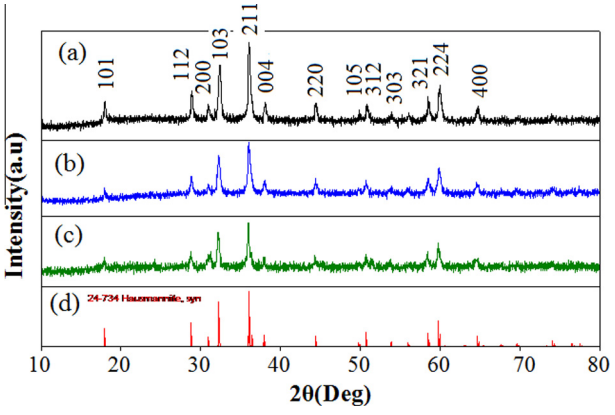

Figure 1 (a) XRD patterns of Mn_3O_4 nanostructures (a) nanobelts, (b) nanosheets, (c) nanoparticles and (d) the standard data from JCPDS card No. 024-0734.

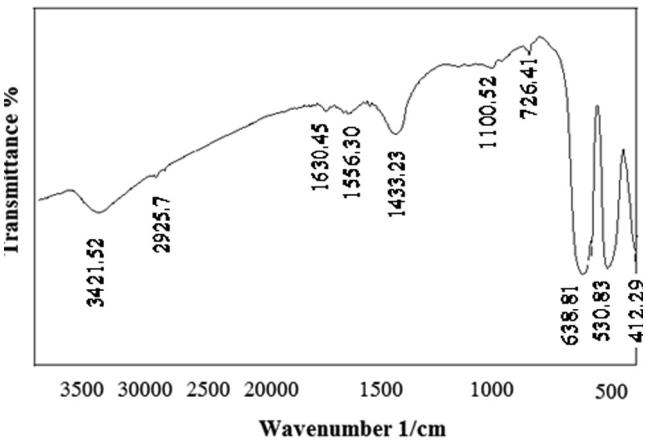

Figure 2 FT-IR spectrum of Mn_3O_4 nanobelts by solvothermal process at 200 °C for 10 h.

Herein, in this paper, we evaluate the reflux and solvothermal methods for the synthesis of Mn_3O_4 nanobelts. The effects of reaction time, melamine and solvent ratio on the formation of final product were estimated. The degradation of diphenylthiocarbazone was investigated by Mn_3O_4 nanobelts based on oxygen pumping and visible light irradiation. Both UV/vis and GC/MS were employed to monitor the temporal course of catalytic reaction.

2. Experimental section

$Mn(acetate)_2{\cdot}H_2O$ was obtained from Sinopharm Chemical Reagent Co., Ltd., melamine was received from Sinphar Chemical Reagent Co., China. All other chemicals in this work were of analytical grade and used without any further treatment. In a typical synthesis, $Mn(CH_3COO)_2{\cdot}H_2O$ (0.7 mmol), melamine (1 mmol) and ethanol:water (70:30%) were stirred for several minutes, and then the mixture was mixed dropwise by adding KOH (0.08 mmol) under magnetic stirring for few minutes. Afterward, the mixture was placed into a round-bottom flask, rigged with condenser and refluxed at 80 °C for 2 h. The obtained solution was transferred into a 40 ml teflon-lined stainless-steel autoclave and heated to 200 °C for 10 h. The autoclave was cooled to room temperature naturally,

Please cite this article in press as: Ahmed, K.A.M., Huang, K. Formation of Mn_3O_4 nanobelts through the solvothermal process and their photocatalytic property. Arabian Journal of Chemistry (2014), http://dx.doi.org/10.1016/j.arabjc.2014.08.014

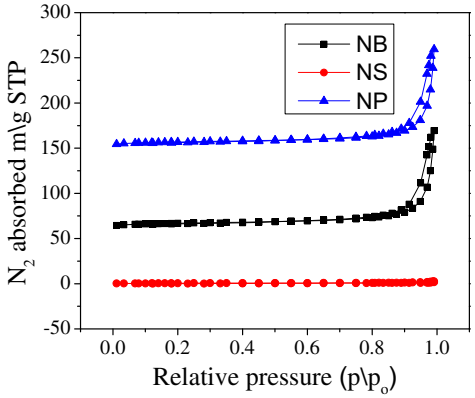

Figure 3 N_2 adsorption–desorption curve of Mn_3O_4 nanobelts, nanosheets and nanoparticles.

and the brown precipitated powders were separated by centrifugation, washed with anhydrous ethanol several times, dried in a vacuum at 50 °C for 12 h, collected for characterization.

2.1. Characterization

The crystal phase of product was examined on an X-ray diffractometer (Panalytical X'Pert Pro; Netherlands) using a Cu Ka target (λ = 1.5418 Å). A FT-IR spectrum was obtained on an EQUINOX55 Bruker FT spectrometer employing a KBr beam splitter. The morphologies and nanostructures of the synthesized products were characterized using a field emission scanning electron microscopy (FEI Sirion 200, Netherlands), transmission electron microscopy (TEM) images collected using a Tecnai $G^2$20, Netherlands and high-resolution transmission electron microscopy (HR-TEM) images were carryout on a JEM-2010 FEF TEM. The surface area and pore size of the product were examined by N_2 isotherms on ASAP 2020 (Micromeritics Co., USA) at liquid nitrogen temperature. A UV–vis spectrophotometer (Shimadzu, model No. 2450) was employed to study the optical properties. All the measurements were carried out at room temperature.

2.2. Catalytic instrumentation

The degradation of diphenylthiocarbazone process was adopted as the probe molecule to evaluate the photocatalytic activity of the as-papered samples. 200 mL of diphenylthiocarbazone (0.2 g/L) solution and 0.02 mmol of the as-prepared catalyst were placed in a three neck glass reactor (250 mL) equipped with a reflux condenser under air bubbling, magnetic stirring and visible light (mercury lamp, GYZ220–230 V, 250 W, Philips Electronics, with a cutoff filter λ > 400 nm) at 60–70 °C. Air as oxygen source was pumped by an air pump. The pH values were controlled by the use of 10% HCl. During the irradiation, 5–6 mL aliquots were sampled at given time intervals. After removing the catalytic powder, the absorbances of the diphenylthiocarbazone solution were analyzed by using a UV–vis spectrophotometer (Shimadzu, model No. 2450). The degree of degradation was calculated from this relation:

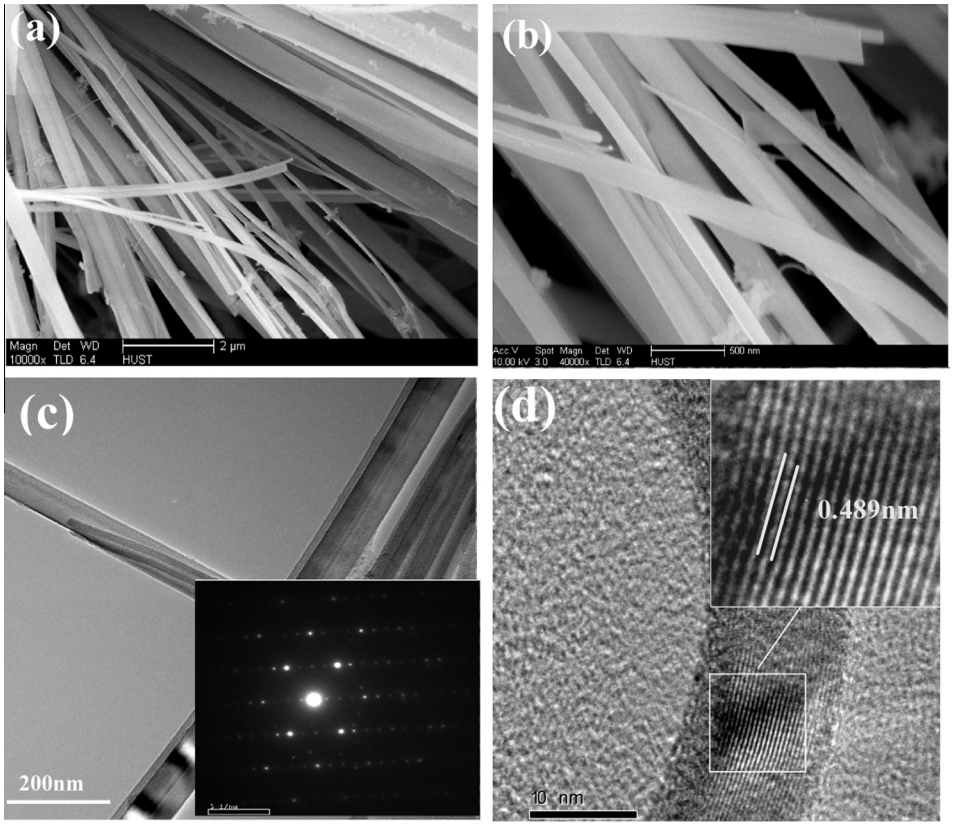

Figure 4 (a) Low- (b) and high-magnification SEM images, (c) TEM images (insert a SE-ED) and (d) HR-TEM images of Mn_3O_4 nanobelts prepared by solvothermal process at 200 °C for 10 h.

Please cite this article in press as: Ahmed, K.A.M., Huang, K. Formation of Mn_3O_4 nanobelts through the solvothermal process and their photocatalytic property. Arabian Journal of Chemistry (2014), http://dx.doi.org/10.1016/j.arabjc.2014.08.014

$$D\% = \frac{A_o - A_t \times 100\%}{A_o}$$

2.3. GC–MS analysis

After reaction, the catalytic powder was removed through filter paper and centrifuged to analysis by GC–MS spectrum with an Agilent 7890A/5975C, equipped with a HP-5-MS capillary column 30 m × 250 μm × 0.25 μm film thickness using a stationary phase of 5% phenyl-methyl poly siloxane. The injector temperature was maintained at 250 °C. For liquid injections (1 μL) the apparatus was run in split mode (1:5) at the flow rate of 3 ml/min.

3. Results and discussion

3.1. Structure and morphology

XRD patterns of the as-fabricated samples by solvothermal process in different amounts of 0, 1 and 2 mmol melamine at 200 °C for 10 h were observed. XRD pattern of the as-obtained Mn_3O_4 nanobelts is shown in Fig. 1(a), reveals that all the diffraction peaks can be exclusively indexed as the tetragonal phase structured Mn_3O_4 with a lattice constant of a = 5.76 Å and c = 9.47 Å and space group of I41/amd; which is in good agreement with the standard data JCPDS card No. 24-0734 (Fig. 1(d)). As presented in Fig. 1(b), the XRD pattern of Mn_3O_4 particles was prepared by solvothermal approach in the absence of melamine. The diffraction peaks could be attributed to the tetragonal of Mn_3O_4 hausmannite (JCPDS card No. 24-0734). Fig. 1(c) is a typical XRD spectrum of as-synthesized sheet- like Mn_3O_4 nanocrystals by melamine amount of 2 mmol, planed all diffraction profiling the same card number of Mn_3O_4 nanobelts and nanoparticles.

The chemical composition of Mn_3O_4 nanobelts was also examined by FTIR measurements. Fig. 2 shows the characteristic absorption bands at 412.29, 530.83, 638.81 and 726.41 cm^{-1} are assigned the stretching modes between the MnO stretching modes of tetrahedral and octahedral sites (Al Sagheer et al., 1999; Wang et al., 2002). Analogously, there were interactions between organic molecules and nanobelts. The bands at 1433.23 and 1556.3 cm^{-1} could be described to the C–H bending vibrations and absorption at 1100.52 cm^{-1} matches the C–N stretching. The broad bands centered at 1630.45, 3421.52 and 2925.7 cm^{-1} are assigned to the O–H stretching and bending modes of water.

Specific surface area of the as-prepared samples was characterized by nitrogen adsorption–desorption isotherm measurements. Fig. 3 shows the nitrogen sorption isotherms curves of pure Mn_3O_4 nanostructures. It can be observed from figure, the nitrogen adsorption–desorption isotherms of the samples are of type IV (Brunauer–Deming–Deming–Teller (BDDT) classification) with two hysteresis loops (Sing et al., 1985). BET surface area of Mn_3O_4 nanobelts is 42.13 m^2/g, which is more than 2.2 and 8.4 times of that of Mn_3O_4 nanosheets and Mn_3O_4 nanoparticles.

The evolution of as-prepared product morphology upon reflux and solvothermal methods was examined by FE-SEM analysis. As shown in Figs. 4(a) and (b), the precursor sample

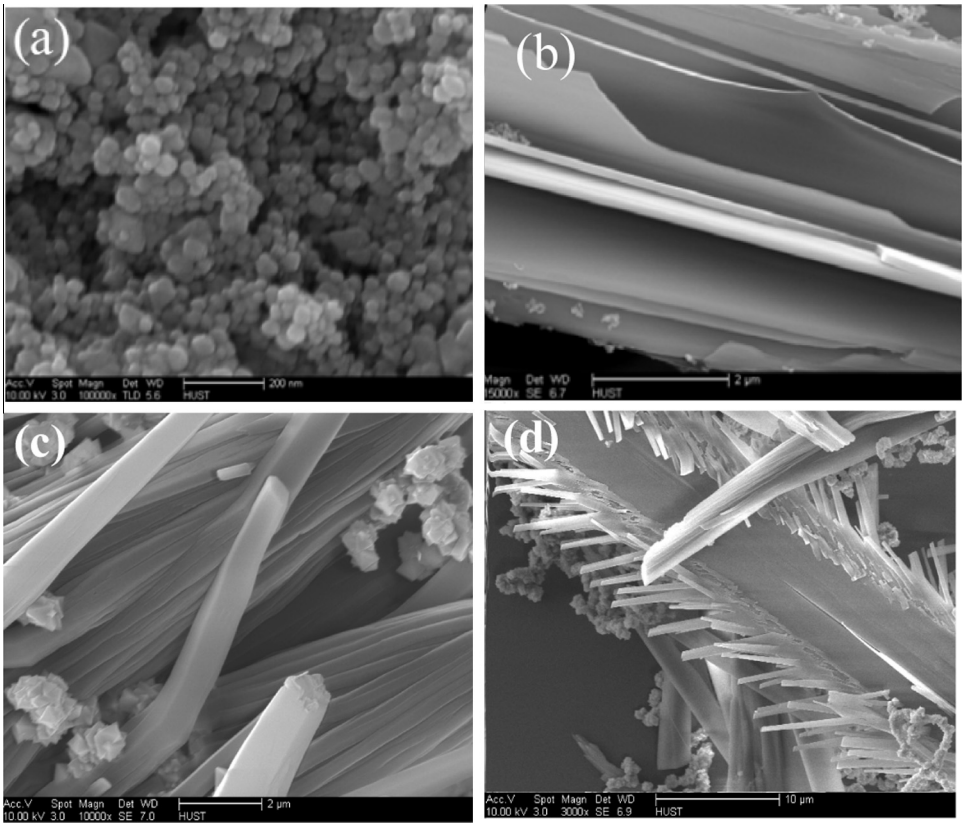

Figure 5 FE-SEM images of products prepared at 200°C (a) without melamine; (b) 2 mmol melamine; (c) water:ethanol volume ratio (10:90 (v/v)) and (d) 1 mmol melamine for 20 h.

Please cite this article in press as: Ahmed, K.A.M., Huang, K. Formation of Mn_3O_4 nanobelts through the solvothermal process and their photocatalytic property. Arabian Journal of Chemistry (2014), http://dx.doi.org/10.1016/j.arabjc.2014.08.014

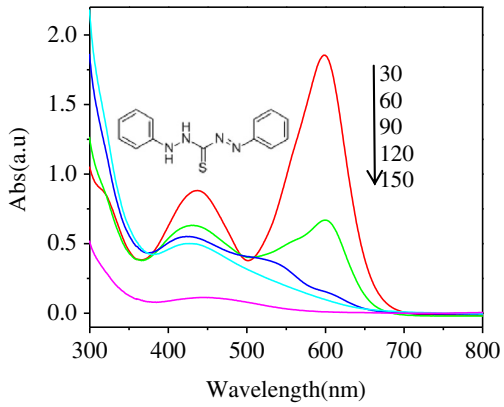

Figure 6 (a) UV–vis spectra of photodegradation of diphenylthiocarbazone by Mn_3O_4 nanobelts.

consists of uniform shape, smooth and flat surfaces nanobelts with a diameter of 100–150 nm and lengths of several micrometers. More detailed studies of the as-prepared sample were examined by TEM. As shown in Fig. 4(c), each product is composed of nanobelts. The dimension of the nanobelts is in good agreement with the estimated value from the FE-SEM results. The corresponding SA-ED pattern of an individual Mn_3O_4 nanobelt (insert a Fig. 4(c)) shows the single-crystalline structure. As presented in Fig. 4(d), the formation of single-crystalline 1D-nanobelts is evidenced from the observation of well-aligned lattice lines in the HR-TEM images. The interplanar distance calculated from the lattice fringes of sample is 0.493 nm, which corresponds to the {1 0 1} plane of tetragonal Mn_3O_4.

To shed light on the formation process of Mn_3O_4 nanobelt, several experimental tests were carried out under different conditions and the intermediate products were inspected by FE-SEM image. From synthesis system it is observed that, the melamine ligand has great effects on the morphology of the final nanobelt. When melamine was canceled under the same conditions, the morphology of the final nanobelts was changed and the smaller nanoparticles with diameter of 40–70 nm were obtained(Fig. 5(a)). When the dosage of melamine was varied from 1 to 2 mmol, the sheet-like microstructures with length of 6 μm and width of 1.5 μm are observed (Fig. 5(b)). Besides the above material, the impacts of solvent ratio and reaction time on Mn_3O_4 nanobelts are also considered. Fig. 5(c) displays the SEM images of the as-grown Mn_3O_4 microrods synthesized by altering ethanol–water volume percentage from 70:30 to 90:10. The width average size of microrods is about 1.5 μm and length is around 10 μm. This morphology not only can be obtained by a changing solvent approach, but also that the growth mechanism can be investigated with other microcrystals by extending the reaction time from 10 to 20 h (Fig. 5(d). According to experimental data, the chemical reactions to obtain as synthesized nanobelts may be formulated as follows:

$$Mn(CH_3COO)_2 + 2KOH \rightarrow Mn(OH)_2 + 2CH_3COOK$$

$$Mn^{+2} + nC_3N_6H_6 \leftrightarrow Mn(C_3N_6H_6)_n^{2+} \quad (n = 1-4)$$

$$6Mn^{+2} + O_2 + 12OH^- \rightarrow 2Mn_3O_4 + H_2O$$

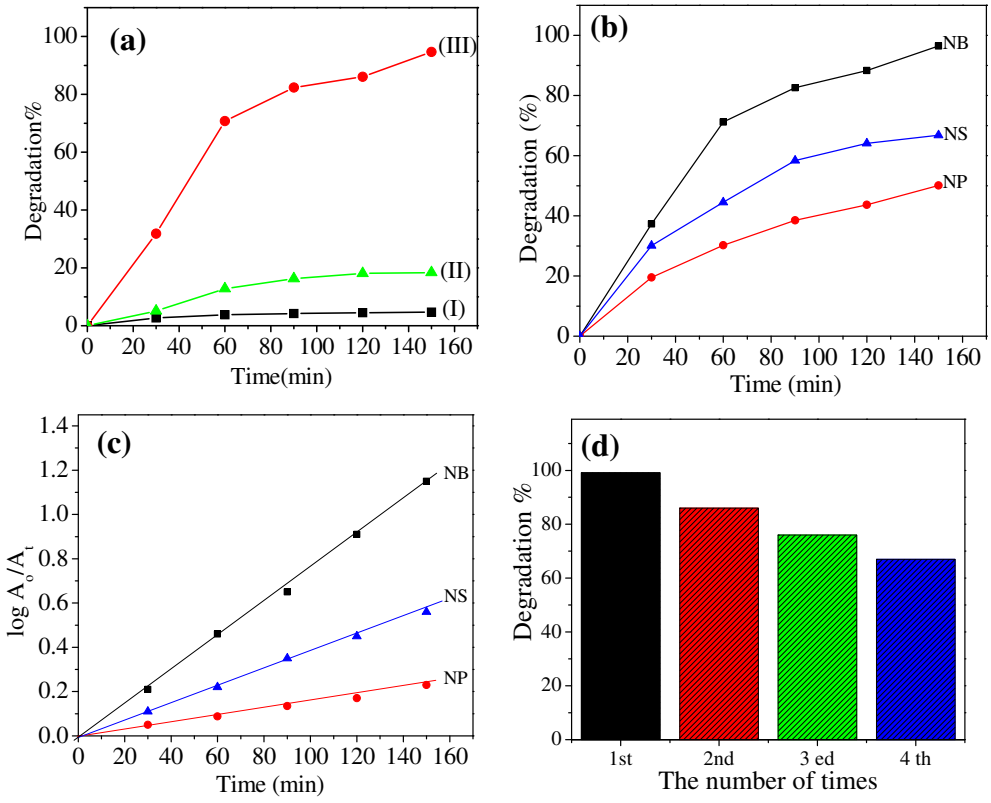

Figure 7 (a) The degradation percentage of diphenylthiocarbazone with (I) O_2, (II) Mn_3O_4 nanobelts and (III) O_2 + Mn_3O_4 nanobelts; (b) the degradation percentage of diphenylthiocarbazone catalyzed by Mn_3O_4 nanostructures; (c) the rate of degradation diphenylthiocarbazone catalyzed by Mn_3O_4 nanostructures; (d) the stability of catalyst after following for four times under visible-light irradiation.

Please cite this article in press as: Ahmed, K.A.M., Huang, K. Formation of Mn_3O_4 nanobelts through the solvothermal process and their photocatalytic property. Arabian Journal of Chemistry (2014), http://dx.doi.org/10.1016/j.arabjc.2014.08.014

Coordination compound of manganese melaminate might play a role in controlling not only release velocity of Mn^{2+} ions, but also growth direction of Mn_3O_4 nanobelts. Recently, the effects of some organic capping ligand on formation of Sb_2O_3, t-Se Fe_3O_4, MoO_3, β-Ga_2O_3 and In_2O_3 nanobelts were reported (Zhang et al., 2004; Ma et al., 2005; Li et al., 2009; Hassan et al., 2010; Abdullah et al., 2013; Amirhoseiny et al., 2013). We believe that excessive melamine as the ligands were adsorbed on surfaces of nanobelts and played a role of capping agent, suppressing the growth rate of one dimension. The building block of the Mn_3O_4 nanobelt, grows along {1 0 1}, with side surfaces prepared from partial Mn^{+2} oxidation intoMn^{+3}due to limited existence of oxygen in the autoclave under such basic condition.

3.2. Catalytic performing

The catalytic activity of Mn_3O_4 nanobelts was evaluated by degrading diphenylthiocarbazone under visible light irradiation at 60–70 °C. Whereas adjustment of pH to 3–4. Two main characteristic absorption bands of dye are displayed by UV–vis spectrum (Fig. 6). One absorbance peak at 600 nm reveals $n \rightarrow \pi^*$ transition of C═N, N═N, C═S groups are contributed to color dye solution and is always used to monitor the decolorization of diphenylthiocarbazone dye. The peak absorbed at 259 nm displays the $\pi \rightarrow \pi^*$ transition in aromatic ring group representing aromatic content of dye. The decrease in both absorbance peaks during catalytic process with irradiation times, suggested that the diphenylthiocarbazone was gradually reduced to minor species.

Moreover, the degradation percentages of diphenylthiocarbazone by Mn_3O_4 nanobelts catalyst or in the absence of catalyst or oxygen air bubbles have presented in Fig. 7(a). Without catalysts, the dye is hardly degraded even under light irradiation and air bubbles for 160 min (curves I). In contrast, it undergoes little or no breakdown of diphenylthiocarbazone dye within Mn_3O_4 nanobelts employees and air pumping privation (curves II). This result suggests the surface area of catalyst and O_2 air are necessary for removal of dye from wastewater, but the oxygen air bubble rate has not significant effect on the degradation process. However, the high value of the decomposition rate of the dye ~99% can be obtained by Mn_3O_4 nanobelts catalyst powder and O_2 air pumping (curve (III). It can also compare of this value other catalytic degradation powders by Mn_3O_4 sheet-like or Mn_3O_4 nanoparticles (Fig. 7(b)), observably, the degradation of dye by Mn_3O_4 nanobelts is best. The reaction of degradation diphenylthiocarbazone rate can be considered pseudo first order. Fig. 7(c) illustrates the plot of log (A_o/A_t) versus times (R^2 = 0.9974). The rate constant may be evaluated as: [k = 2.303log

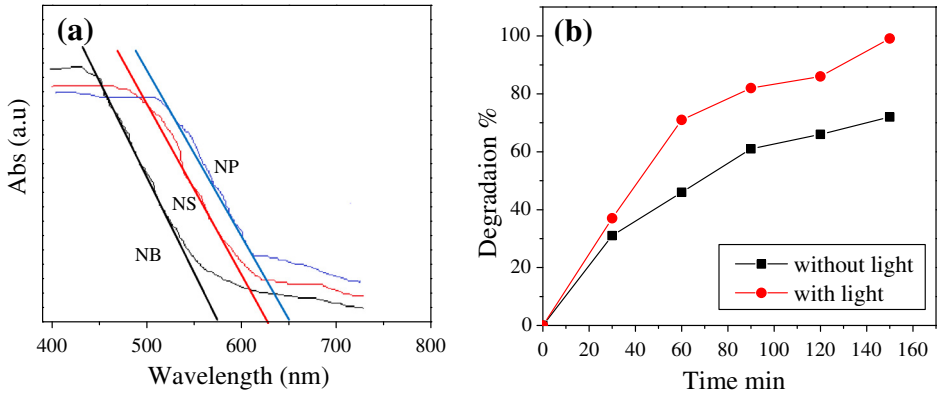

Figure 8 (a) The diffuse reflectance spectrum of the as-prepared materials Mn_3O_4 nanobelts (NB), Mn_3O_4nanosheets (NS) and Mn_3O_4nanoparticles (NP); (b) The degradation efficiency of diphenylthio-carbazone by Mn_3O_4 nanobelts with and without light irradiation.

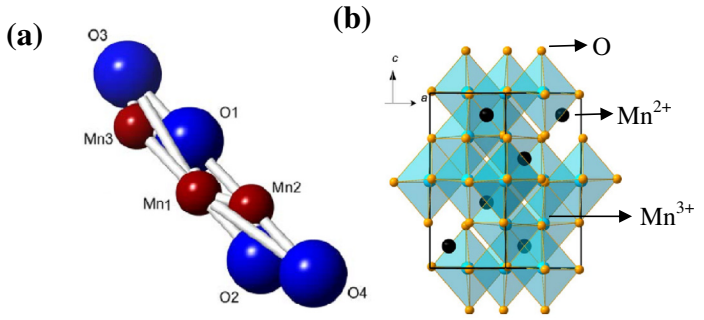

Figure 9 (a) Crystal Maker Demo displays an anisotropic structure of Mn_3O_4 nanobelts and (b) The black spheres are tetrahedrally coordinated Mn^{2+} on the A site and the cyan spheres are the octahedrally coordinated Mn^{3+} on the B site. Orange spheres are O.

$(A_o/A_t)/t]$; from this plot, the rate constant (k) is about 1.544×10^{-2} min. This value is higher than the catalytic reaction by sheet-like Mn_3O_4 nanocrystals or Mn_3O_4 nanoparticles. On the other hand, the reuse stability of Mn_3O_4 nanobelts catalyst is presented in Fig. 7(d). The diphenylthiocarbazone degradation activity of four reuses was 99.1%, 86.5%, 76.3% and 66.8%, after 150 min of reaction and at 70 °C, respectively. The result reveals the catalytic efficiency of the catalyst has a slight decrease after each cycle. The reason may be partly due to inescapable loss during the recovery of the catalyst and lacking some of its adsorption ability.

3.3. Degradation mechanism

Fig. 8(a) shows the diffused reflectance spectra of Mn_3O_4 samples. From the results in figure, one can observed that the absorption edges of Mn_3O_4 nanobelts, Mn_3O_4 sheet-like and Mn_3O_4 nanoparticles are about 560, 625 and 650 nm, respectively. The band gap (Eg) of the samples can be calculated from the following equation: $[Eg_{(eV)} = 1420/\lambda_{(nm)}]$ (Yang et al., 2010). From this relation, the band gap energies of Mn_3O_4 nanobelts, Mn_3O_4 sheet-like and Mn_3O_4 nanoparticles are about 2.22, 1.98 and 1.91 eV, respectively. It was recently

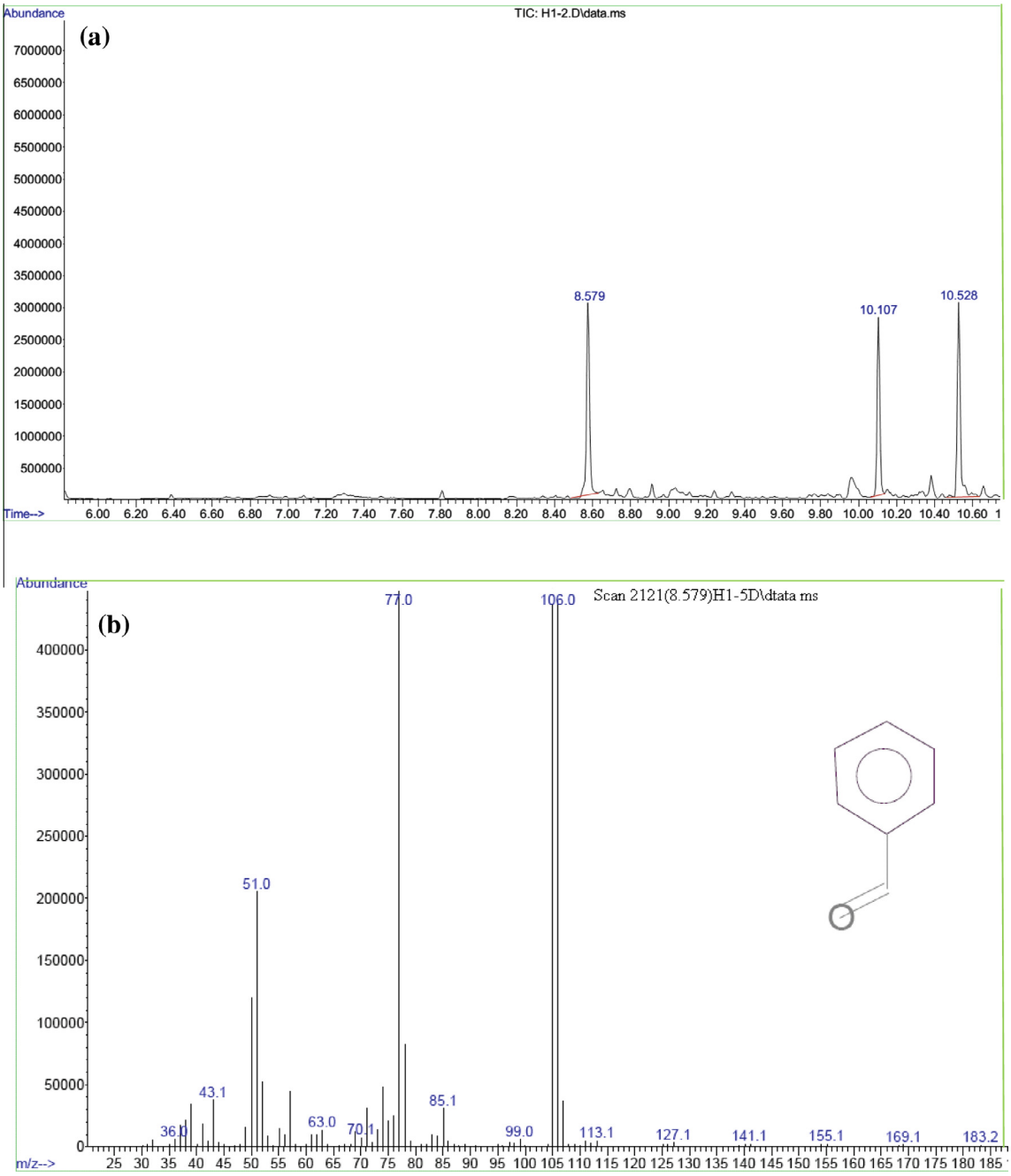

Figure 10 The GC and MS spectra of degradation products of diphenylthio-carbazone with Mn_3O_4 nanobelts and O_2 under light irradiation; (a) GC spectrum of degradation products; (b–d) Mass-specters of benzaldehyde, 4-tert-butylbenzoic acid and N-benzylbenzamide.

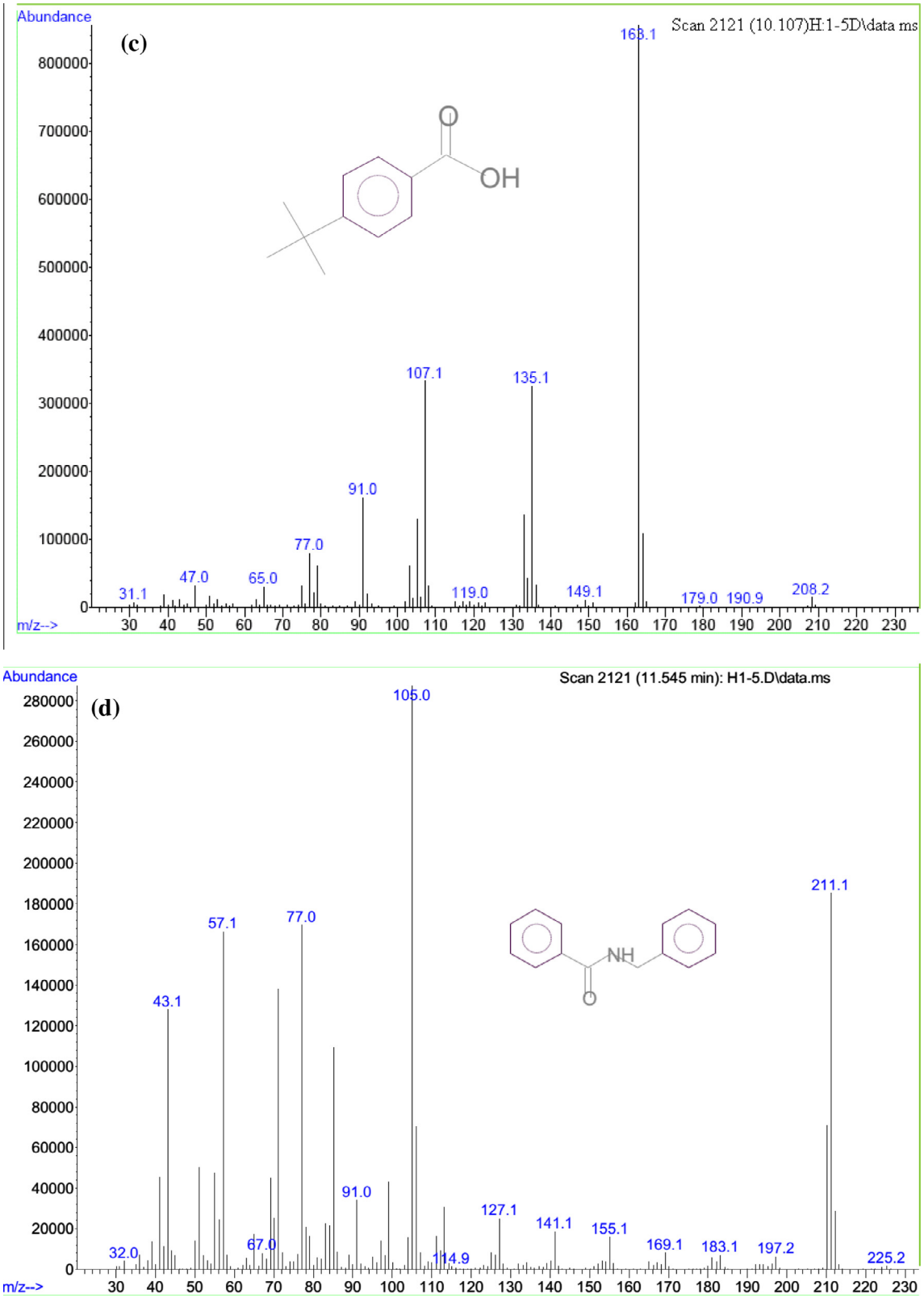

Fig. 10 (*continued*)

reported that the large band gap as an important in ban the electron–hole recombination and ultimately enhances the photocatalytic efficacy. The increase in band gap led to efficient charge separation and it reduced the rate of recombination of the electro-hole pair and enhanced the rapid electron transfer at the solid–liquid interface (Kumaresan et al., 2010). Similar to our present results, the photocatalytic activity of Mn_3O_4 nanobelts has high absorbance of light in the visible

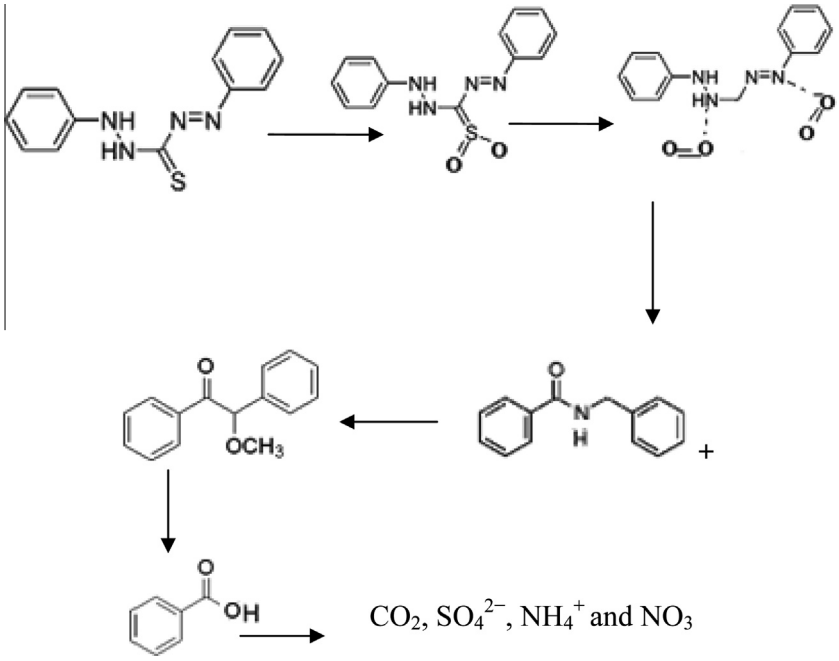

Figure 11 Photocatalytic degradation pathway of diphenylthiocarbazone dye by Mn_3O_4 nanobelts, under air pumping and visible light irradiation.

region and high optical band gap absorption, indicating applicability as an absorbing of this material than other Mn_3O_4 sheet-like and Mn_3O_4 nanoparticles. Due to increase in the band gap energy and spinal structure with the Mn^{2+} cations in the tetrahedral sites and the Mn^{3+} cations in the octahedral sites, $Mn_1^{2+}[Mn_2^{3+}]O_4^{2-}$ (Fig. 9) and being derived from the cubic spinel through a strong Jahn–Teller distortion (Tackett et al., 2007; Raj et al., 2010; Rohani and Entezari, 2010), Mn_3O_4 nanobelts exhibited enhanced photocatalytic activity. The role of light irradiation in the catalytic degradation of diphenyl-thiocarbazone over Mn_3O_4 nanobelts is shown in Fig. 8(b). The degradation efficiency of catalyst is considerably higher in the same condition with light irradiation than that of the degradation of dye in absence of light.

The evaluation of the degradation effectiveness of diphenylthiocarbazone catalyzed by Mn_3O_4 nanobelts was carried out through GC–MS spectroscopy. The main degradation compounds were identified by MS (Fig. 10). Based on the identified byproducts, the reaction pathways of diphenylthiocarbazone degradation were proposed, as postulated in Fig. 11. Due to the above results and previous reports in refers (Rauf and Ashraf, 2009; Rhadfi et al., 2010; Ahmed et al., 2011), the large number of main reactive oxygen species including h^+, $\cdot O_2^-$ and $\cdot OH$ involved in photocatalytic process may be responsible for degradation dye. There are no useful methods for detecting hydroxyl radicals. The reason is the high reactivity of these radicals which will react in terephthalic acid and it has shown to be impossible to introduce sufficient concentrations of an indicator into cells to react preferentially with hydroxyl radicals. So as per our observation, the photo-holes are certainly not concerned by the initial step since the reactant is cationic and not an electron donor. By contrast, the free radical oxygenations can attack the C=S and N=N functional group in diphenylthiocarbazone, which is probably adsorbed perpendicularly to the surface down to the final products of CO_2, SO_4^{2-}, NH_4^+ and NO_3^- (tested the end of catalytic reaction by $Ba(OH)_2$ and glass rod moistened of HCl).

4. Conclusions

In conclusion, we synthesized Mn_3O_4 nanostructure with various morphologies such as nanobelt nanosheets and nanoparticles by reflux and solvothermal routes. Melamine amounts, solvent ratios and reaction time played important role in the formation of the as-prepared products. The optical studies showed direct band gap energy of 19.1–2.21 eV. Due to energy band gap and surface area, the Mn_3O_4 nanobelts exhibited better catalytic activity of diphenylthiocarbazone degradation than Mn_3O_4 nanosheets and nanoparticles. The decomposition reaction of dye follows first order kinetics and as analyzed by GC–MS and shows the dye solution was degraded into small species. All results suggest the strong O_2-activating ability of Mn_3O_4 nanobelts showed promising applications in the oxidative degradation of diphenylthiocarbazone under visible-light irradiation.

Acknowledgements

We thank the Taif University, Al-Neelain University and faculty from the Analysis and Test Center of Huazhong University of Science and Technology for the technical assistance on characterization. This research was supported by MOST 973 program (Project No. 2006CB705606a).

References

Abdullah, Q.N., Yam, F.K., Hassan, Z., Bououdina, M., 2013. Growth and conversion of β-Ga_2O_3 nanobelts into GaN nanowires via catalyst-free chemical vapordeposition technique. Superlattices Microstruct. 54, 215–224.

Ahmad, T., Ganguly, A., Ahmed, J., Ganguli, A.K., Alhartomy, O.A.A., 2011. Nanorods of transition metal oxalates: a versatile route to the oxide nanoparticles. Arabian J. Chem. 4, 125–134.

Ahmadi, T.S., Wang, Z.L., Green, T.C., Henglein, A., Elsayed, M.A., 1996. Shape controlled synthesis of colloidal platinum nanoparticles. Science 272, 1924–1926.

Ahmed, K.A.M., Peng, H., Wu, K.B., Huang, K.X., 2011. Hydrothermal preparation of nanostructured manganese oxides (MnO_x) and their electrochemical and photocatalytic properties. Chem. Eng. J. 172, 531–539.

Al Sagheer, F.A., Hasan, M.A., Pasupulety, L., Zaki, M.I., 1999. Low-temperature synthesis of hausmannite Mn_3O_4. J. Mater. Sci. Lett. 18, 209–211.

Amirhoseiny, M., Hassan, Z., ShaShiong, N., 2013. Synthesis of nanocrystalline In_2O_3 on different Si substrates at wet oxidation environment. Optik 124, 2679–2681.

Armstrong, A.R., Bruce, P.G., 1996. Synthesis of layered $LiMnO_2$ as an electrode for rechargeable lithium batteries. Nature 381, 499–500.

Bai, Z., Fan, N., Ju, Z., Guo, C., Qian, Y., Tang, B., Xiong, S., 2013. Facile synthesis of mesoporous Mn_3O_4 nanotubes and their excellent performance for lithium-ion batteries. J. Mater. Chem. A 1, 10985–10990.

Baldi, M., Finocchio, E., Milella, F., Busca, G., 1998. Catalytic combustion of C3 hydrocarbons and oxygenates over Mn_3O_4. Appl. Catal. B: Environ. 16, 43–51.

Chowdhury, A.-N., Azam, M.S., Aktaruzzaman, M., Rahim, A., 2009. Oxidative and antibacterial activity of Mn_3O_4. J. Hazard. Mater. 172, 1229–1235.

Comini, E., Faglia, G., Sberveglieri, G., Calestani, D., Zanotti, L., Zha, M., 2005. Tin oxide nanobelts electrical and sensing properties. Sens. Actuators B111–112, 2–6.

Dong, Y., Yang, H., He, K., Song, S., Zhang, A., 2009. β-MnO_2 nanowires: a novel ozonation catalyst for water treatment. Appl. Catal. B: Environ. 85, 155–161.

Du, C., Yun, J., Dumas, R.K., Yuan, X., Liu, K., Browning, N.D., Pan, N., 2008. Three-dimensionally intercrossing Mn_3O_4 nanowires. Acta Mater. 56, 3516–3522.

Fang, X., Hu, L., Huo, K., Gao, B., Zhao, L., Liao, M., Chu, P.K., Bando, Y., Golberg, D., 2011a. New ultraviolet photodetector based on individual Nb_2O_5 nanobelts. Adv. Funct. Mater. 21, 3907–3915.

Fang, X., Wu, L., Hu, L., 2011b. ZnS nanostructure arrays: a developing material star. Adv. Mater. 23, 585–598.

Grootendorst, E., Verbeek, Y., Ponce, V., 1995. The role of the Mars and Van Krevelen mechanism in the selective oxidation of nitrosobenzene and the deoxygenation of nitrobenzene on oxidic catalysts. J. Catal. 157, 706–712.

Han, S., Hu, L., Gao, N., Al-Ghamdi, A.A., Fang, X., 2014. Efficient self-assembly synthesis of uniform CdS spherical nanoparticles-Au nanoparticles hybrids with enhanced photoactivity. Adv. Funct. Mater. 24, 3725–3733.

Hassan, M.F., Guo, Z.P., Chen, Z., Liu, H.K., 2010. Carbon-coated MoO_3 nanobelts as anode materials for lithium-ion batteries. J. Power Sources 195, 2372–2376.

Huang, M.H., Mao, S., Feick, H., Yan, H.Q., Wu, Y.Y., Kind, H., Weber, E., Russo, R., Yang, P.D., 2001. Room-temperature ultraviolet nanowire nanolasers. Science 292, 1897–1899.

Kumaresan, L., Mahalakshmi, M., Palanichamy, M., Murugesan, V., 2010. Synthesis, characterization, and photocatalytic activity of Sr^{2+} doped TiO_2 nanoplates. Ind. Eng. Chem. Res. 49, 1480–1485.

Lee, N.R., Jung, H., 2012. Low-temperature fabrication of Mn_3O_4 nanorods by solid-state decomposition of exfoliated MnO_2 nanosheets. J. Phys. Chem. Solids 73, 1473–1477.

Li, D., Wu, X., Xiao, T., Tao, W., Yuan, M., Hu, X., Yang, P., Tang, Y., 2012. Hydrothermal synthesis of mesoporous Co_3O_4 nanobelts by means of a compound precursor. J. Phys. Chem. Solids 73, 169–175.

Li, L., Chu, Y., Liu, Y., Wang, D., 2009. Solution-phase synthesis of single-crystalline Fe_3O_4 magnetic nanobelts. J. Alloys Compd. 472, 271–275.

Li, N., Wang, J.-Y., Liu, Z.-Q., Guo, Y.-P., Wang, D.-Y., Su, Y.-Z., Chen, S., 2014. One-dimensional ZnO/Mn_3O_4 core/shell nanorod and nanotube arrays with high supercapacitive performance for electrochemical energy storage. RSC Adv. 4, 17274–17281.

Ma, Y., Qi, L., Shen, W., Ma, J., 2005. Selective synthesis of single-crystalline selenium nanobelts and nanowires in micellar solutions of nonionic surfactants. Langmuir 21, 6161–6164.

Mai, L.Q., Lao, C.S., Hu, B., Zhou, J., Qi, Y.Y., Chen, W., Gu, E.D., Wang, Z.L., 2006. Synthesis and electrical transport of single crystal $NH_4V_3O_8$ nanobelts. J. Phys. Chem. B110, 18138–18141.

Mo, M.S., Zeng, J.H., Liu, X.M., Yu, W.C., Zhang, S.Y., Qian, Y.T., 2002. Controlled hydrothermal synthesis of thin single-crystal tellurium nanobelts and nanotubes. Adv. Mater. 14, 1658–1662.

Pan, Z.W., Dai, Z.R., Wang, Z.L., 2001. Nanobelts of semiconducting oxides. Science 291, 1947–1949.

Peng, L., Hu, L., Fang, X., 2014. Energy harvesting for nanostructured self-powered photodetectors. Adv. Funct. Mater. 24, 2591–2610.

Raj, M.E.A., Victoria, G.S., Bena, J.V., Ravidhas, C., Wollschler, J., Suendorf, M., Neumann, M., Jayachandran, M., Sanjeeviraja, C., 2010. XRD and XPS characterization of mixed valence Mn_3O_4 hausmannite thin films prepared by chemical spray pyrolysis technique. Appl. Surf. Sci. 256, 2920–2926.

Rauf, M.A., Ashraf, S.S., 2009. Radiation induced degradation of dyes-an overview. J. Hazard. Mater. 166, 6–16.

Rhadfi, T., Piquemal, J.-Y., Sicard, L., Herbst, F., Briot, E., Benedetti, M., Atlamsani, A., 2010. Polyol-made Mn_3O_4 nanocrystals as efficient fenton-like catalysts. Appl. Catal. A: General 386, 132–139.

Rohani, B.T., Entezari, M.H., 2010. Sonosynthesis of Mn_3O_4 nanoparticles in different media without additives. Chem. Eng. J. 164, 261–266.

Shao, C., Guan, H., Liu, Y., Li, X., Yang, X., 2004. Preparation of Mn_2O_3 and Mn_3O_4 nanofibers via an electrospinning technique. J. Solid State Chem. 177, 2628–2631.

Shen, Y.F., Zerger, P., Deguzman, R.N., Suib, S.L., Mccurdy, L., Potter, D.I., O'Young, C.L., 1993. Manganese oxide octahedral molecular sieves: preparation, characterization, and applications. Science 260, 511–515.

Sing, K.S.W., Everett, D.H., Haul, R.A.W., Moscou, L., Pierotti, R.A., Rouquerol, J., Siemieniewska, T., 1985. Reporting physisorption data for gas/solid systems with special reference to the determination of surface area and porosity. Pure Appl. Chem. 57, 603–619.

Song, J., Wang, X., Riedo, E., Wang, Z., 2005. Elastic property of vertically aligned nanowires. Nano Lett. 5, 1954–1958.

Song, R., Feng, S., Wang, H., Hou, C., 2013. Effect of organic solvents on particle size of Mn_3O_4 nanoparticles synthesized by a solvothermal method. J. Solid State Chem. 202, 57–60.

Stobhe, E.R., Boer, B.A.D., Geus, J.W., 1999. The reduction and oxidation behaviour of manganese oxides. Catal. Today 47, 161–167.

Tackett, R., Lawes, G., Melot, B.C., Grossman, M., Toberer, E.S., Seshadri, R., 2007. Magnetodielectric coupling in Mn_3O_4. Phys. Rev. B 76, 024409–024415.

Tan, Y., Meng, L., Peng, Q., Li, Y., 2011. One-dimensional single-crystalline Mn_3O_4 nanostructures with tunable length and magnetic properties of Mn_3O_4 nanowires. Chem. Commun. 47, 1172–1174.

Wang, J., Sun, J., Bao, Y., Bian, X., 2003. Novel way to synthesize Mn_3O_4 nanobelts via oriented attachment. J. Mater. Sci. Technol. 19, 489–491.

Wang, W., Xu, C., Wang, G., Liu, Y., Zheng, C., 2002. Preparation of smooth single crystal. Mn_3O_4 nanowires. Adv. Mater. 14, 837–840.

Wang, Z.H., Geng, D.Y., Zhang, Y.J., Zhang, Z.D., 2008. Morphology, structure and magnetic properties of single-crystal Mn_3O_4 nanorods. J. Cryst. Growth 310, 4148–4151.

Please cite this article in press as: Ahmed, K.A.M., Huang, K. Formation of Mn_3O_4 nanobelts through the solvothermal process and their photocatalytic property. Arabian Journal of Chemistry (2014), http://dx.doi.org/10.1016/j.arabjc.2014.08.014

Wang, Z.L., 2004. Functional oxide nanobelts: materials, properties and potential applications in nanosystems and biotechnology. Annu. Rev. Phys. Chem. 55, 159–255.

Williams, F.A., Nozik, J., 1984. Solid-state perspectives of the photoelectrochemistry of semiconductor electrolyte junction. Nature 312, 21–27.

Xia, Y.N., Yang, P.D., Sun, Y.G., Wu, Y.Y., Mayers, B., Gates, B., Yin, Y.D., Kim, F., Yan, H.Q., 2003. One-dimensional nanostructures: synthesis, characterization and applications. Adv. Mater. 15, 353–389.

Xiao, Z.L., Han, C.Y., Kwok, W.K., Wang, H.H., Welp, U., Wang, J., Crabtree, G.W., 2004. Tuning the architecture of mesostructures by electrodeposition. J. Am. Chem. Soc. 126, 2316–2317.

Yang, X., Ma, F., Xu, L., Guo, Y., Guo, Y., Huo, M., 2010. Mixed phase titania nanocomposites codoped with metallic silver and vanadium oxide: new visible/UV-light-driven photocatalyst for dye degradation. J. Hazard. Mater. 175, 429–438.

Yu, Y., Tang, S., Wang, R., Shi, Y., Nie, B., Zhai, L., Zhang, X., Du, Y., 2008. Synthesis of single-crystalline barium dititanate nanobelts. Cryst. Growth Des. 8, 1481–1483.

Zhang, Y., Li, G., Zhang, J., Zhang, L., 2004. Shape-controlled growth of one-dimensional Sb_2O_3 nanomaterials. Nanotechnology 15, 762–765.

Zhang, Q., Liu, Y., Duan, Y., Fu, N., Liu, Q., Fang, Y., Sun, Q., Lin, Y., 2014. Mn_3O_4/graphene composite as counter electrode in dye-sensitized solar. RSC Adv. 4, 15091–15097.

Zwinkels, M.F.M., Jaras, S.G., Menon, P.G., Griffik, T.A., 1993. Catalytic materials for high-temperature combustion. Catal. Rev. Sci. Eng. 35, 319–358.

Please cite this article in press as: Ahmed, K.A.M., Huang, K. Formation of Mn_3O_4 nanobelts through the solvothermal process and their photocatalytic property. Arabian Journal of Chemistry (2014), http://dx.doi.org/10.1016/j.arabjc.2014.08.014